

4D Model-Based Iterative Reconstruction from Interlaced Views

K. Aditya Mohan*, S. V. Venkatakrishnan[¶], John W. Gibbs[†], E. Begum Gulsoy[†], Xianghui Xiao[‡],
M. De Graef[§], Peter W. Voorhees[†], and Charles A. Bouman*

*School of Electrical and Computer Engineering, Purdue University, West Lafayette, IN 47907, USA

[†]Department of Materials Science and Engineering, Northwestern University, Evanston, IL 60208-3108, USA

[‡]Argonne National Laboratory, Lemont, IL 60439

[§]Department of Materials Science and Engineering, Carnegie Mellon University, Pittsburgh, PA 15213.

[¶]Advanced Light Source, Lawrence Berkeley National Laboratory, Berkeley, California 94720, USA

Abstract—X-ray tomography is increasingly being used for 4D spatio-temporal imaging of material samples at micron and finer scales. However, the temporal resolution of widely used 4D reconstruction methods is severely limited by the need to acquire a very large number of views for each reconstructed 3D volume. In this paper, we present a time interlaced model-based iterative reconstruction (TIMBIR) method which can significantly improve the temporal resolution of reconstructions. TIMBIR is a synergistic combination of two innovations. The first innovation, interlaced view sampling, is a novel approach to data acquisition which distributes the view angles more evenly in time. The second innovation is a 4D model based iterative reconstruction algorithm (MBIR) which can produce time resolved volumetric reconstructions of the sample from the interlaced views. Reconstructions of simulated data indicate that TIMBIR can improve the temporal resolution by an order of magnitude relative to existing approaches.

I. INTRODUCTION

Four-dimensional computed tomography (4D-CT) using synchrotron X-rays is enabling scientists to study a wide variety of physical processes [1], [2] in the material sciences. However, in-situ 4D synchrotron imaging still remains a major challenge owing to limitations on the data acquisition rate [1]. The traditional approach to 4D-CT is to acquire a sequence of parallel beam projections of the object, which is rotated at a constant speed, at progressively increasing equi-spaced view angles (henceforth called progressive view sampling). Typically, the projections in each π radians rotation are grouped together and reconstructed into a single 3D volume using an analytical reconstruction algorithm such as filtered back projection (FBP) [3], [4] or Fourier domain reconstruction methods [5]–[7]. Since the number of views required for Nyquist spatial sampling is approximately the number of sampled pixels in the sensor’s cross-axial field of view [3], the data acquisition rate becomes a limiting factor on the

K. A. Mohan, S. V. Venkatakrishnan, E. B. Gulsoy, M. De Graef, P. W. Voorhees and C. A. Bouman were supported by an AFOSR/MURI grant #FA9550-12-1-0458. J. W. Gibbs was supported by a DOE NNSA Stewardship Science Graduate Fellowship (Grant No. DE-FC52-08NA28752). Use of the Advanced Photon Source, an Office of Science User Facility operated for the U.S. Department of Energy (DOE) Office of Science by Argonne National Laboratory, was supported by the U.S. DOE under Contract No. DE-AC02-06CH11357. This research was supported in part through computational resources provided by Information Technology at Purdue, West Lafayette, Indiana.

temporal resolution of the reconstructions. In order to increase the temporal resolution, either the number of projections per rotation can be reduced or the range of view angles used for reconstruction can be decreased. However, in both the cases the signal is under sampled and analytic reconstruction algorithms produce substantial artifacts [3], [8]–[10].

In order to improve the quality of reconstruction, several new sampling strategies based on optimal Nyquist sampling [11]–[15], compressed sensing [16], and other techniques [17], [18] have been proposed for other tomographic applications. An alternate approach to improving reconstructions is to use more advanced model-based iterative reconstruction (MBIR) methods [19]–[22], which are based on the estimation of a reconstruction which best fits models of both the sensor measurements (i.e., the forward model) and the object (i.e., prior model). In the context of medical CT, several authors have also shown that modeling the temporal correlations [23]–[27] in addition to modeling the spatial correlations improves the quality of 4D MBIR reconstructions.

In this paper, we propose an approach to 4D reconstruction of time varying objects, which we call time interlaced model based iterative reconstruction (TIMBIR). TIMBIR is the synergistic combination of a novel interlaced view sampling technique and a 4D MBIR algorithm. In the new interlaced view sampling method, all the views that are typically acquired over half a rotation using progressive view sampling are instead acquired over multiple half-rotations. In order to reconstruct the data acquired using this technique, we propose a new 4D MBIR algorithm. In addition to modeling the measurement noise and spatio-temporal correlations in the 4D object, the MBIR algorithm reduces ring and streak artifacts by modeling the detector non-idealities [28], [29] and measurement outliers caused by high energy photons (called “zingers”) [21]. We adapt our forward model introduced in [21] for synchrotron tomography to the current 4D framework and combine it with a modified qGGMRF [30] based prior model and formulate the MBIR cost function.

II. INTERLACED VIEW SAMPLING IN TOMOGRAPHY

In order to achieve Nyquist sampling for each 3D volume in synchrotron X-ray tomography, it is typically necessary to collect $N_\theta = N_p$ progressive views where N_p is the number

of sampled pixels perpendicular to the axis of rotation. In the traditional approach, all N_θ progressive views are taken in sequence while the sample is rotated continuously over π radians (see Fig. 1(a)). The object is then reconstructed at a temporal rate of $F_s = F_c/N_\theta$ where F_c is the data acquisition rate.

In contrast to the traditional approach, we propose an interlaced view sampling method where each frame of data consisting of N_θ distinct views are acquired over K interlaced sub-frames as shown in Fig. 1(b). Each sub-frame of data then consists of N_θ/K equally spaced views, but together the full frame of data contains all N_θ distinct views of the object. For a continuously rotating object, the formula describing the view angle as a function of the discrete sample index, n , is given by

$$\theta_n = \left[nK + \mathcal{B}_r \left(\left\lfloor \frac{nK}{N_\theta} \right\rfloor \bmod K \right) \right] \frac{\pi}{N_\theta}, \quad (1)$$

where K is a power of 2, $b = \mathcal{B}_r(a)$ is the bit-reverse function which takes the binary representation of the integer a and reverses the order of the bits to form the output b [31]. Thus, in interlaced view sampling all the distinct N_θ views are acquired over a $K\pi$ radians rotation of the object. This requires spinning the object at K times the typical rotation speed while maintaining the same data acquisition rate. The object is then reconstructed at a temporal rate of $F_s = rF_c/N_\theta$ by reconstructing r time samples every frame. In TIMBIR, we typically set the parameter r equal to the number of sub-frames, K .

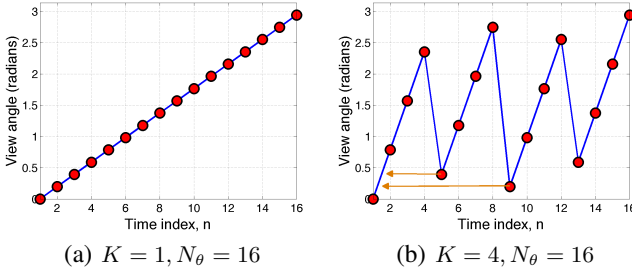


Fig. 1. Illustration of interlaced view sampling pattern for different values of K . (a,b) are plots of $\theta_n \bmod(\pi)$ vs. time index, n , for $K = 1$ and $K = 4$. The arrows show the relative difference between the angular values across sub-frames for the interlaced data acquisition scheme.

III. FORMULATION OF MBIR COST FUNCTION

In synchrotron X-ray tomography, we typically reconstruct the attenuation coefficients of the object from the acquired data. In order to reconstruct the object, we use the MBIR framework. The MBIR reconstruction is given by the iterative minimization of the following optimization problem,

$$\left(\hat{x}, \hat{\phi} \right) = \underset{x, \phi}{\operatorname{argmin}} \{ -\log p(y|x, \phi) - \log p(x) \}, \quad (2)$$

where $p(y|x, \phi)$ is the pdf of the projection data, y , given the reconstruction, x , and the unknown system parameters, ϕ , and $p(x)$ is a pdf for the 4D object.

A. Measurement Model

We begin by deriving a likelihood function $p(y|x, \phi)$ for the projection data, y , from a time varying object, x . We model each voxel of the object as an independent piecewise constant function in time such that there are r equi-length reconstruction time samples in each frame. Thus, the projections ranging from $(j-1)N_\theta/r + 1$ to jN_θ/r are assumed to be generated from the j^{th} time sample. The vector of attenuation coefficients of the object at the j^{th} time sample is denoted by x_j .

Using the synchrotron X-ray tomography model we introduced in [21], if $\lambda_{n,i}$ is the measurement at the i^{th} detector element and n^{th} view and if $\lambda_{D,i}$ is the measurement in the absence of the sample, then an estimate of the projection integral is given by $y_{n,i} = \log \left(\frac{\lambda_{D,i}}{\lambda_{n,i}} \right) - d_i$ where d_i is an unknown offset error. Let $\beta_{T,\delta}(z)$ be the generalized Huber function [21] of the form

$$\beta_{T,\delta}(z) = \begin{cases} z^2 & |z| < T \\ 2\delta T |z| + T^2(1-2\delta) & |z| \geq T. \end{cases} \quad (3)$$

where δ and T are parameters of the Huber function. In our model, the parameters of the generalized Huber function are chosen such that $0 < \delta < 1$ and $T > 0$. The Huber function is non-convex in this range of parameter values. If we denote y to be the vector of all projections, $y_{n,i}$, x to be the vector of attenuation coefficients at all time steps, then by adapting the 3D forward model presented in [21] to 4D we obtain the following likelihood function,

$$\begin{aligned} -\log p(y|x, d, \sigma) = & \\ \frac{1}{2} \sum_{j=1}^L \sum_{n=n_{j-1}}^{n_j-1} \sum_{i=1}^M \beta_{T,\delta} \left((y_{n,i} - A_{n,i,*} x_j - d_i) \frac{\sqrt{\Lambda_{n,i,i}}}{\sigma} \right) & \\ + ML \frac{N_\theta}{r} \log(\sigma) + c(y), & \quad (4) \end{aligned}$$

where $n_j = j \frac{N_\theta}{r} + 1$, L is the total number of time samples in the reconstruction, $A_{n,i,*}$ is the i^{th} row of the forward projection matrix A_n , Λ_n is a diagonal matrix modeling the noise statistics, M is the total number of detector elements, and $c(y)$ is a constant that will be ignored in the subsequent optimization. The variance of the projection measurement, $y_{n,i}$, is inversely proportional to the mean photon count and hence we set $\Lambda_{n,i,i} = \lambda_{n,i}$ [32]. Since, typically $\lambda_{n,i}$ is not equal to the photon count but is proportional to the photon count, there exists an unknown constant of proportionality σ such that $\frac{\lambda_{n,i}}{\sigma^2}$ is the inverse variance of the projection measurement, $y_{n,i}$.

B. Prior Model

We use a q-generalized Gaussian Markov random field (qGGMRF) [30] based prior model for the voxels. The prior model is used to regularize the reconstruction in time as well as space. Using this model, the logarithm of the density function

of x is given by

$$\begin{aligned}
-\log p(x) &= \sum_{j=1}^L \sum_{\{k,l\} \in \mathcal{N}} w_{kl} \rho_s(x_{j,k} - x_{j,l}) \\
&+ \sum_{k=1}^P \sum_{\{j,i\} \in \mathcal{T}} \tilde{w}_{ji} \rho_t(x_{j,k} - x_{i,k}) + \text{constant}, \quad (5)
\end{aligned}$$

$$\text{where } \rho_s(\Delta) = \frac{\Delta_t \Delta_s^3 \left| \frac{\Delta}{\Delta_s \sigma_s} \right|^2}{c_s + \left| \frac{\Delta}{\Delta_s \sigma_s} \right|^{2-p}}, \quad \rho_t(\Delta) = \frac{\Delta_t \Delta_s^3 \left| \frac{\Delta}{\Delta_t \sigma_t} \right|^2}{c_t + \left| \frac{\Delta}{\Delta_t \sigma_t} \right|^{2-p}},$$

and $x_{j,k}$ is the k^{th} voxel of the object at time sample j , P is the total number of voxels in each 3D time sample, \mathcal{N} is the set of all pairwise cliques in 3D space (all pairs of neighbors in a 26 point spatial neighborhood system), \mathcal{T} is the set of all pairs of indices of adjacent time samples (2 point temporal neighborhood system), p , c_s , c_t , σ_s and σ_t are qGGMRF parameters, Δ_s is a parameter proportional to the side length of a voxel and Δ_t is a parameter proportional to the duration of each time sample in the reconstruction. The weight parameters are set such that $w_{kl} \propto |k-l|^{-1}$, $\tilde{w}_{ji} \propto |j-i|^{-1}$, and normalized so that $\sum_{l \in \mathcal{N}_k} w_{kl} + \sum_{i \in \mathcal{T}_j} \tilde{w}_{ji} = 1$, where \mathcal{N}_k is the set of all spatial neighbors and \mathcal{T}_j is the set of all temporal neighbors of voxel $x_{j,k}$. The terms Δ_s and Δ_t in the prior model ensure invariance of the prior to changing voxel size [33].

C. MBIR Cost Function

By substituting (4) and (5) into (2), we get the following cost function,

$$\begin{aligned}
c(x, d, \sigma) &= MLN_\theta \log(\sigma)/r \\
&+ \frac{1}{2} \sum_{j=1}^L \sum_{n=n_j-1}^{n_j-1} \sum_{i=1}^M \beta_{T,\delta} \left((y_{n,i} - A_{n,i,*} x_j - d_i) \frac{\sqrt{\Lambda_{n,i,i}}}{\sigma} \right) \\
&+ \sum_{j=1}^L \sum_{\{k,l\} \in \mathcal{N}} w_{kl} \rho_s(x_{j,k} - x_{j,l}) + \sum_{k=1}^P \sum_{\{j,i\} \in \mathcal{T}} \tilde{w}_{ji} \rho_t(x_{j,k} - x_{i,k}). \quad (6)
\end{aligned}$$

The reconstruction is obtained by jointly minimizing the cost, $c(x, d, \sigma)$, with respect to x , d and σ . Additionally we constraint $\sum_{i=1}^M d_i = 0$, to prevent any shift in the estimated value of the reconstruction.

IV. OPTIMIZATION ALGORITHM

The cost function (6) is in general non-convex in x , d and σ . Minimizing the current form of the cost function given by (6) is computationally expensive. So, we instead adapt the functional substitution based optimization algorithm in [21] to efficiently minimize the current form of the cost function (6). Our method also ensures monotonic decrease of the cost function (6).

We also implemented the non-homogeneous iterative coordinate descent (NHICD) [19] for the voxel updates and a multi-resolution initialization method to improve the convergence speed of the algorithm. To prevent the algorithm from

converging to a local minimum, we do not update the offset error, d_i , and variance parameter, σ , at the coarsest scale of multi-resolution.

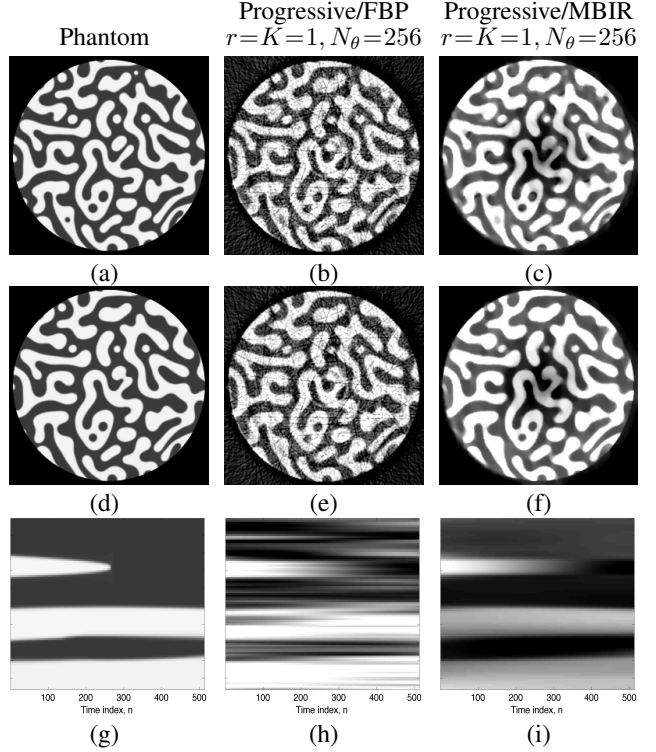


Fig. 2. Reconstructions of a progressive view dataset using FBP and MBIR. The first and second rows show a 2D slice of the object in the $u-v$ plane at different times. The third row shows a v -axis slice of the object vs. time. The first column (a,d,g) shows the phantom. Reconstruction ($r=1$) of a progressive view dataset with $N_\theta = 256$ using FBP is shown in the second column (b,e,h) and using MBIR is shown in the third column (c,f,i). Reconstruction of rapidly time-varying objects using conventional methods results in poor temporal resolution.

V. EXPERIMENTAL RESULTS

In this section, we compare FBP and MBIR reconstructions of simulated datasets using both the traditional progressive view sampling and the proposed interlaced view sampling methods. First, a time varying phantom (see Fig. 2 (a,d,g)) in 4D is generated using the Cahn-Hilliard equation [34] which models the process of phase separation in the cross-axial plane ($u-v$ axes). The phantom is representative of the phenomenon that we are interested in studying in 4D. The two phases of the object have attenuation coefficients of 2.0 mm^{-1} and 0.67 mm^{-1} respectively. The phantom is assumed to have a voxel resolution of $0.65 \times 0.65 \times 0.65 \text{ } \mu\text{m}^3$ and a size of $16 \times 1024 \times 1024$. The phantom is then sampled in time at the data acquisition rate, F_c , and the projections are generated by forward projecting the sampled phantom at the appropriate angles. To simulate detector non-idealities in a synchrotron measurement system, we add an offset error d_i to the projection $y_{n,i}$ at every n^{th} view. To simulate the effect of zingers, we randomly set 0.1% of the projections, y , to zero. The simulated value of the variance parameter is $\sigma^2 = 10$.

The simulated sensor has a resolution of $N_p = 256$ pixels in the cross-axial direction and 4 pixels in the axial direction. The reconstruction has a size of $4 \times 256 \times 256$ voxels and a spatial resolution of $2.6 \times 2.6 \times 2.6 \mu\text{m}^3$. The temporal reconstruction rate is $F_s = rF_c/N_\theta$ where r is the number of reconstruction time samples in a frame, F_c is the data rate, and N_θ is the number of distinct views. For computing the root mean square error (RMSE) between the reconstruction and the high resolution phantom, the reconstructions are up sampled in time to the data rate F_c using cubic interpolation. Also, since the phantom has higher spatial resolution than the reconstructions, the phantom is down-sampled by averaging over blocks of pixels to the reconstruction resolution before comparison. The regularization parameters in the prior model are chosen such that they minimize the RMSE between the reconstruction and the phantom. We set $p = 1.2$, $\delta = 0.1$ and $T = 4$. The algorithm stops when the percentage change in average magnitude of voxel updates is less than 0.1%.

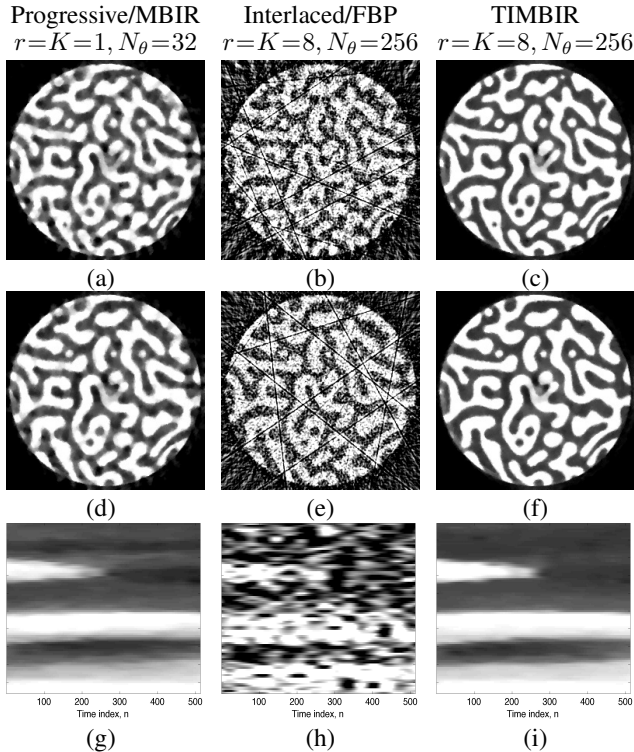


Fig. 3. TIMBIR vs. other methods for high temporal resolution reconstruction. The first and second rows show a 2D slice of the object in the $u-v$ plane at different times. The third row shows a v -axis slice of the object vs. time. The first column (a,d,g) shows the MBIR reconstructions ($r = 1$) of progressive views with $N_\theta = 32$. Reconstruction ($r = 8$) of interlaced views with $K = 8$, $N_\theta = 256$ using FBP is shown in the second column (b,e,h), and TIMBIR is shown in the third column (c,f,i).

The traditional approach to 4D synchrotron tomography is to use progressive view sampling and an analytic reconstruction algorithm such as FBP. So, we generate a dataset of progressive views with $N_\theta = 256$ and reconstruct it at a rate of $F_s = F_c/256$ by reconstructing $r = 1$ volumetric time sample every frame. The reconstruction using FBP is shown in Fig.

TABLE I
RMSE BETWEEN THE RECONSTRUCTION AND THE PHANTOM.
RECONSTRUCTION USING TIMBIR HAS THE LOWEST RMSE AMONG ALL THE METHODS.

Description	Parameters	RMSE (mm^{-1})
Nyquist Progressive, Slow FBP	$r = 1, K = 1, N_\theta = 256$	0.3376
Nyquist Progressive, Slow MBIR	$r = 1, K = 1, N_\theta = 256$	0.2814
Sub-Nyquist Progressive, Fast MBIR	$r = 1, K = 1, N_\theta = 32$	0.2554
Interlaced, Fast FBP	$r = 8, K = 8, N_\theta = 256$	0.6035
Interlaced, Fast MBIR (TIMBIR)	$r = 8, K = 8, N_\theta = 256$	0.2193

2 (b,e,h) and using MBIR is shown in Fig. 2 (c,f,i). When compared to FBP, MBIR produces lower noise reconstructions with reduced artifacts while preserving the spatial resolution (Fig. 2 (b,e) and Fig. 2 (c,f)). However, from Fig. 2 (h,i) we can also see that neither FBP nor MBIR are able to reconstruct temporal edges accurately.

Next, we investigate different methods of increasing temporal resolution. First, we reduce the number of progressive view angles to $N_\theta = 32$ and reconstruct it at a rate of $F_s = F_c/32$ using MBIR ($r = 1$). However, due to the severe under sampling of views the MBIR reconstruction suffers from severe loss in quality (Fig. 3 (a,d,g)). This illustrates that merely reducing the number of views in every π radians rotation and using an advanced reconstruction algorithm is insufficient for our problem. Next, we generate a dataset of interlaced views in which each frame of $N_\theta = 256$ angles is interlaced over $K = 8$ sub-frames. We then reconstruct it at a rate of $F_s = F_c/32$ by reconstructing $r = 8$ time samples every frame. Thus, this reconstruction has 8 times the temporal resolution of the conventional approach. The reconstruction using FBP is shown in Fig. 3 (b,e,h), and TIMBIR is shown in Fig. 3 (c,f,i). Thus, we can see that reconstructing the interlaced views with FBP results in extremely poor quality reconstruction (Fig. 3 (b,e)). In contrast, TIMBIR with interlaced views results in a substantially better reconstruction of the object with minimal artifacts (Fig. 3 (c,f)). Furthermore, we can see that TIMBIR is able to more accurately reconstruct temporal edges (Fig. 3 (i)) than any other method (Fig. 3 (g,h) and Fig. 2 (h,i)). The RMSE between the reconstructions and the ground-truth shown in Table I support these visual conclusions. Thus, TIMBIR with its synergistic combination of interlaced sampling and MBIR reconstruction, results in a much higher quality reconstruction than either method can achieve by itself. The run time of the TIMBIR reconstruction algorithm was 46.6 minutes using 16 processor cores.

VI. CONCLUSION

In this paper, we propose a novel interlaced view sampling approach which when combined with a 4D MBIR algorithm was able to achieve a synergistic improvement in reconstruction quality for synchrotron X-ray CT. By comparing reconstructions of simulated data using different methods we showed that TIMBIR can improve temporal resolution by an order of magnitude relative to existing approaches.

REFERENCES

- [1] D. Rowenhorst and P. Voorhees, "Measurement of interfacial evolution in three dimensions," *Annual Review of Materials Research*, vol. 42, no. 1, pp. 105–124, 2012.
- [2] L. K. Aagesen, J. L. Fife, E. M. Lauridsen, and P. W. Voorhees, "The evolution of interfacial morphology during coarsening: A comparison between 4D experiments and phase-field simulations," *Scripta Materialia*, vol. 64, no. 5, pp. 394–397, 2011.
- [3] A. C. Kak and M. Slaney, *Principles of Computerized Tomographic Imaging*. Philadelphia, PA: Society for Industrial and Applied Mathematics, 2001.
- [4] J. Hsieh, *Computed Tomography: Principles, Design, Artifacts, and Recent Advances*. SPIE Press, Nov. 2009.
- [5] D. Gottlieb, B. Gustafsson, and P. Forssen, "On the direct Fourier method for computer tomography," *Medical Imaging, IEEE Transactions on*, vol. 19, no. 3, pp. 223–232, 2000.
- [6] F. Marone and M. Stampanoni, "Regridding reconstruction algorithm for real-time tomographic imaging," *Journal of Synchrotron Radiation*, vol. 19, no. 6, pp. 1029–1037, Nov 2012.
- [7] J. Walden, "Analysis of the direct Fourier method for computer tomography," *Medical Imaging, IEEE Transactions on*, vol. 19, no. 3, pp. 211–222, 2000.
- [8] M. Bertram, J. Wiegert, D. Schafer, T. Aach, and G. Rose, "Directional view interpolation for compensation of sparse angular sampling in cone-beam CT," *Medical Imaging, IEEE Transactions on*, vol. 28, no. 7, pp. 1011–1022, 2009.
- [9] R. R. Galigekere, K. Wiesent, and D. W. Holdsworth, "Techniques to alleviate the effects of view aliasing artifacts in computed tomography," *Medical Physics*, vol. 26, no. 6, 1999.
- [10] M. Davison, "The ill-conditioned nature of the limited angle tomography problem," *SIAM Journal on Applied Mathematics*, vol. 43, no. 2, pp. 428–448, 1983.
- [11] P. Rattey and A. G. Lindgren, "Sampling the 2-D radon transform," *Acoustics, Speech and Signal Processing, IEEE Transactions on*, vol. 29, no. 5, pp. 994–1002, 1981.
- [12] A. Faridani and L. R. Erik, "High-resolution computed tomography from efficient sampling," *Inverse Problems*, vol. 16, no. 3, p. 635, 2000.
- [13] A. M. Cormack, "Sampling the radon transform with beams of finite width," *Physics in Medicine and Biology*, vol. 23, no. 6, p. 1141, 1978.
- [14] N. Willis and Y. Bresler, "Optimal scan for time-varying tomography I: Theoretical analysis and fundamental limitations," *Image Processing, IEEE Transactions on*, vol. 4, no. 5, pp. 642–653, 1995.
- [15] —, "Optimal scan for time-varying tomography II: Efficient design and experimental validation," *Image Processing, IEEE Transactions on*, vol. 4, no. 5, pp. 654–666, 1995.
- [16] Y. Kaganovsky, D. Li, A. Holmgren, H. Jeon, K. P. MacCabe, D. G. Politte, J. A. O'Sullivan, L. Carin, and D. J. Brady, "Compressed sampling strategies for tomography," *J. Opt. Soc. Am. A*, vol. 31, no. 7, pp. 1369–1394, Jul 2014.
- [17] J. Miao, F. Frster, and O. Levi, "Equally sloped tomography with oversampling reconstruction," *Physical Review B*, vol. 72, no. 5, p. 052103, 2005, pRB.
- [18] Z. Zheng and K. Mueller, "Identifying sets of favorable projections for few-view low-dose cone-beam CT scanning," in *11th International Meeting on Fully Three-Dimensional Image Reconstruction in Radiology and Nuclear Medicine*, 2011.
- [19] Z. Yu, J. Thibault, C. Bouman, K. Sauer, and J. Hsieh, "Fast model-based X-ray CT reconstruction using spatially nonhomogeneous ICD optimization," *IEEE Trans. on Image Processing*, vol. 20, no. 1, pp. 161–175, Jan. 2011.
- [20] S. V. Venkatakrishnan, L. F. Drummy, M. A. Jackson, M. De Graef, J. Simmons, and C. A. Bouman, "A model based iterative reconstruction algorithm for high angle annular dark field-scanning transmission electron microscope (HAADF-STEM) tomography," *Image Processing, IEEE Transactions on*, vol. 22, no. 11, pp. 4532–4544, 2013.
- [21] K. Mohan, S. Venkatakrishnan, L. Drummy, J. Simmons, D. Parkinson, and C. Bouman, "Model-based iterative reconstruction for synchrotron X-ray tomography," in *Acoustics, Speech and Signal Processing (ICASSP), 2014 IEEE International Conference on*, May 2014, pp. 6909–6913.
- [22] S. J. Kisner, E. Haneda, C. A. Bouman, S. Skatter, M. Kourinny, and S. Bedford, "Limited view angle iterative CT reconstruction," *Proc. SPIE*, vol. 8296, pp. 82 960F–82 960F–9, 2012.
- [23] H. Wu, A. Maier, R. Fahrig, and J. Hornegger, "Spatial-temporal total variation regularization (STTVR) for 4D-CT reconstruction," *Proc. SPIE*, vol. 8313, pp. 83 133J–83 133J–7, 2012. [Online]. Available: <http://dx.doi.org/10.1117/12.911162>
- [24] L. Ritschl, S. Sawall, M. Knaup, A. Hess, and M. Kachelriess, "Iterative 4D cardiac micro-CT image reconstruction using an adaptive spatio-temporal sparsity prior," *Physics in Medicine and Biology*, vol. 57, no. 6, p. 1517, 2012.
- [25] X. Jia, Y. Lou, B. Dong, Z. Tian, and S. Jiang, "4D computed tomography reconstruction from few-projection data via temporal non-local regularization," in *Proceedings of the 13th International Conference on Medical Image Computing and Computer-assisted Intervention: Part I*, ser. MICCAI'10. Berlin, Heidelberg: Springer-Verlag, 2010, pp. 143–150.
- [26] Z. Tian, X. Jia, B. Dong, Y. Lou, and S. B. Jiang, "Low-dose 4DCT reconstruction via temporal nonlocal means," *Medical Physics*, vol. 38, no. 3, pp. 1359–1365, 2011.
- [27] J. Hinkle, M. Szegedi, B. Wang, B. Salter, and S. Joshi, "4D CT image reconstruction with diffeomorphic motion model," *Medical Image Analysis*, vol. 16, no. 6, pp. 1307–1316, 2012.
- [28] T. Donath, "Quantitative X-ray microtomography with synchrotron radiation," Ph.D. dissertation, GKSS-Forschungszentrum, 2007.
- [29] J. Sijbers and A. Postnov, "Reduction of ring artifacts in high resolution micro-CT reconstructions," *Physics in Medicine and Biology*, vol. 49, no. 14, p. N247, 2004.
- [30] J.-B. Thibault, K. D. Sauer, C. A. Bouman, and J. Hsieh, "A three-dimensional statistical approach to improved image quality for multislice helical CT," *Medical Physics*, vol. 34, no. 11, pp. 4526–4544, 2007.
- [31] R. M. Cramblitt and J. P. Allebach, "Analysis of time-sequential sampling with a spatially hexagonal lattice," *J. Opt. Soc. Am.*, vol. 73, no. 11, pp. 1510–1517, Nov 1983.
- [32] K. Sauer and C. Bouman, "Bayesian Estimation of Transmission Tomograms Using Segmentation Based Optimization," *IEEE Trans. on Nuclear Science*, vol. 39, pp. 1144–1152, 1992.
- [33] S. Oh, A. Milstein, C. Bouman, and K. Webb, "A general framework for nonlinear multigrid inversion," *Image Processing, IEEE Transactions on*, vol. 14, no. 1, pp. 125–140, 2005.
- [34] J. W. Cahn and J. E. Hilliard, "Free energy of a nonuniform system. I. interfacial free energy," *The Journal of Chemical Physics*, vol. 28, no. 2, 1958.